Published in final edited form as:
J Neurol. 2005 September ; 252(9): 1082–1092. doi:10.1007/s00415-005-0819-7.

Metabolic characteristics of cortical malformations causing epilepsy

Susanne G. Mueller, MD[1,2], **Kenneth D. Laxer, MD**[3], **Jerome A. Barakos, MD**[3], **Nathan Cashdollar, BA**[1], **Derek L. Flenniken, BSc., Dr. rer. nat.**[1], **Peter Vermathen**[1], **Gerald B. Matson, PhD**[1,4], and **Michael W. Weiner, MD**[1,2]

[1] Dept. of Veterans Affairs (DVA), Medical Center, Magnetic Resonance Spectroscopy Unit, San Francisco (CA), USA

[2] Dept. of Radiology, University of California, San Francisco (CA), USA

[3] Pacific Epilepsy Program, California Pacific Medical Center, 2100 Webster Street, Suite 115, San Francisco (CA) 94115, USA, Tel.: +1-415/600-7880, Fax: +1-415/600-7885

[4] Dept. of Pharmaceutical Chemistry, University of California, San Francisco (CA), USA

Abstract

Purpose—Cortical malformations (CMs) are increasingly recognized as the epileptogenic substrate in patients with medically refractory neocortical epilepsy (NE). The aim of this study was to test the hypotheses that: 1. CMs are metabolically heterogeneous. 2. The structurally normal appearing perilesional zone is characterized by similar metabolic abnormalities as the CM.

Methods—Magnetic resonance spectroscopic imaging (MRSI) in combination with tissue segmentation was performed on eight patients with NE and CMs and 19 age-matched controls. In controls, NAA, Cr, Cho, NAA/Cr and NAA/Cho of all voxels of a given lobe were expressed as a function of white matter content and thresholds for pathological values determined by calculating the 95% prediction intervals. These thresholds were used to identify metabolically abnormal voxels within the CM and in the perilesional zone.

Results—30% of all voxels in the CMs were abnormal, most frequently because of decreases of NAA or increases of Cho. Abnormal voxels tended to form metabolically heterogeneous clusters interspersed in metabolically normal regions. Furthermore, 15% of all voxels in the perilesional zone were abnormal, the most frequent being decreases of NAA and Cr.

Conclusion—In CMs metabolically normal regions are interspersed with metabolically heterogeneous abnormal regions. Metabolic abnormalities in the perilesional zone share several characteristics of CMs and might therefore represent areas with microscopic malformations and/or intrinsic epileptogenicity.

Keywords

cortical malformation; MR-spectroscopy; NAA; epilepsy

Introduction

Disruption of the developmental processes during neuroblast proliferation and differentiation, neuroblast migration, or postmigrational cortical organization may result in cortical

Correspondence to: Kenneth D. Laxer, laxer@cooper.cpmc.org.

malformations (CM). With the development of high-quality neuroimaging in the last few years, CMs are increasingly being identified in patients suffering from intractable epilepsy [10]. Several electrophysiological and neurohistochemical studies have shown that some CM can possess an intrinsic epileptogenicity [22]. Furthermore, subtle histological and electrophysiological disturbances are sometimes also found in normal appearing tissue surrounding the MRI visible malformation [29]. ^{1}H MR spectroscopy (MRS) is able to identify the neuronal dysfunction/neuron loss associated with epileptic activity by a reduction of the neuronal marker N-acetylaspartate (NAA) [30] even in the absence of structural abnormalities on MRI [11]. Therefore, NAA reductions might also be helpful for a better delineation of structural and functional abnormal regions in CMs and the surrounding normal appearing tissue. This assumption is supported by the fact that the most consistent finding of the limited number of MRS studies in CMs has indeed been a reduction of NAA [6,13,17–19,26,31]. However, considering the fact that MRI visible CMs usually contain abnormal neuronal elements and are characterized by severe disturbances of the histological architecture, metabolic abnormalities are probably not restricted to NAA but affect also creatine/phosphocreatine (Cr) and choline compounds (Cho). Furthermore, CMs can be histopathologically heterogeneous even within an individual lesion [4], and metabolic abnormalities can be expected to reflect this heterogeneity. Therefore, this study used MR spectroscopic imaging (MRSI) and tissue segmentation to test the following two hypotheses: 1. CM are metabolically heterogeneous, i.e., while NAA reductions are probably the most prominent abnormalities, there are also abnormalities of Cr and Cho and these abnormalities show a regional variability within the CM. 2. Metabolic abnormalities are not restricted to macroscopically abnormal regions of the CM, but can also be found in the surrounding normal appearing perilesional tissue, where they show similar characteristics, i.e., metabolic and regional variability, as the CM proper.

Patients and methods

Study Population

The committee of human research at the University of California, San Francisco (UCSF) approved the study, and written informed consent was obtained from each subject according to the Declaration of Helsinki. Patients from the Northern California Comprehensive Epilepsy Center, UCSF, undergoing exploration for epilepsy surgery were included if they fulfilled the following criteria: 1. NE associated with MRI visible CM. 2. Identification of the primary epileptogenic zone with prolonged ictal and interictal Video/EEG/Telemetry. 3. MRSI examinations covering the whole CM or a large part of it. Between 1996 and 2002 eight patients (4 females and 4 males) between 16 and 37 years, mean age 26.3 ± 8.5 years fulfilled these criteria and were thus included into this study. Table 1 displays the clinical characteristics of the patients. All patients had been seizure free for at least 24 hours before the MRSI exam. The control population consisted of 19 age-matched healthy volunteers (11 females and 8 males), between 16 and 46 years, mean age 29.1 ± 8.7 years.

Structural MRI Acquisition

All subjects were scanned on a 1.5 T VISION™ MR system (Siemens Inc., Iselin, NJ). The following sequence of images was acquired: 1. A double spin echo sequence (DSE) (TR/TE1/TE2 = 2500/20/80 ms timing, 1.0 × 1.4 mm^2 in-plane resolution, slice thickness = 3 mm). 2. A volumetric magnetization-prepared rapid gradient echo (MPRAGE) (TR/TE/TI = 13.5/7/300 ms timing, 15° flip angle, 1.0 × 1.0 mm^2 in-plane resolution, slice thickness 1.4 mm). The segmentation procedure used for this study is described in detail elsewhere [21,28]. Briefly, T1, T2 and PD weighted images were coregistered and corrected for inhomogeneity. An automated histogram analysis was employed to select conservative samples of CSF, white and gray matter. Those representative regions were then used to provide starting sets for a K-mean

cluster analysis and each pixel within the brain was assigned to the category with the nearest cluster mean value. In addition to the standard operator-assisted post processing of the segmented images done in our laboratory [25], the interhemispheric fissure, the frontal, temporal, parietal and occipital lobes, insula, brainstem and cerebellum were manually delineated using anatomical landmarks [9], thereby further categorizing cortical gray matter and white matter into left and right frontal cortical gray and white matter, temporal cortical gray and white matter, parietal cortical gray and white matter, occipital gray and white matter and insular gray matter. The CM and, if associated with an abnormal signal, also surrounding white matter or overlaying cortex were identified visually and manually delineated on the T1 orT2 weighted MRI, depending on which it showed best, by an experienced radiologist (BJA). This information was incorporated into the segmented image as "malformation". MRI characteristics were used for classification and determination of type of each CM.

^{1}H MRSI Acquisition and Spectral Processing

Multislice ^{1}H MRSI data (TR/TE = 1800/135 ms, 45 min total acquisition) was acquired from three 15 mm thick slices using slice-selective inversion – recovery (TI = 170 ms) to null the lipid signal and chemical shift selected water suppression (CHESS). The *k*-space sampling was accomplished with 36 × 36 circularly bounded phase encoding steps across a 280 × 280 mm^2 field of view, yielding a nominal voxel size of about 0.9 ml. The patients and controls were studied with two different but for this purpose comparable protocols. From 1996 – March 1997, i.e., for patients No 1–3, and 7 controls, the "bottom" slice was angulated along the long axis of the hippocampus. The other two slices were aligned along the optic nerve: the "middle" slice was positioned to include the corpus callosum and the "top" slice slightly above the corpus callosum ("old protocol"). After March 1997, i.e., for patients No 4–8 and 12 controls, all three slices were angulated along the anterior-posterior axis of the corpus callosum −10°. The "bottom" slice was placed covering the tail of the hippocampus, the "middle" slice right below the inferior aspect of the corpus callosum and the "top" slice slightly above ("new protocol") (cf. Fig. 1). In both protocols, slices were positioned as uniformly as possible, no attempt was made to modify the positioning as to optimize the representation of a CM in the slice. The ^{1}H MRSI data were zero-padded to 64 × 64 points in the spatial domain and from 512 to 1024 points in the spectral domain. Before Fourier reconstruction, the time domain data were 4 Hz Gaussian filtered. Reduction of spurious resonances from extracranial lipids was accomplished by selective k-space extrapolation [14]. A fully automated spectral fitting software package developed in this laboratory [20,27] was used to fit the peak areas of NAA, Cr and Cho. Quality control was ensured by rejecting voxels with NAA peaks that had a smaller than 4 or larger than 9 Hz line width at half peak height and/or fits with residual sum squares that were outside the upper 95 percentile distribution of residuals from all fits. Typically no more than 10–20% of all voxels of the "middle" and "top" slice were rejected by these criteria. However, approximately 70% of all voxels in the frontal lobe region ("new protocol") and 40% of all voxels in temporal lobe region ("old and new protocol") in the "bottom" slice were rejected. The spectral quality in these regions was adversely affected by susceptibility artifacts. The peak areas of NAA, Cr and Cho were corrected for CSF contribution to the voxel and receiver gain and expressed relative to the intensity of median ventricular CSF of each subject as measured from the proton density MRI. Additionally, NAA/Cr and NAA/Cho of each voxel were calculated.

Identification of metabolically abnormal voxels

The segmented MR images were aligned with the MRSI slices, using slice position and orientation information, i.e., each MRSI slice contained the information from the five corresponding segmented MRI slices. The tissue composition for each MRSI voxel was then computed by convolving each tissue map of the segmented MR images with the discrete transform of the MRSI spatial response function and MRSI slice profile including corrections

for chemical shift displacement [25]. The brain regions covered by the MRSI slices were different between the two protocols. Therefore, the following calculations were done for each protocol separately. To determine threshold values for voxels with abnormal metabolite intensities in a lobe, the 95% prediction interval was calculated using all voxels in this lobe of the control group. To this purpose, all voxels from a respective control group containing 50% or more of a lobe, e.g. right frontal lobe or left parietal lobe, were selected. For the insula, which was represented in the two lower MRSI slices in the "new protocol", but not in the "old protocol", voxels with 30% or more insular cortex were selected. These criteria were applied because the so chosen voxels showed an excellent agreement with the corresponding lobes on the segmented image when depicted on the corresponding MRI. Of the selected voxels, those containing more than 15% cerebellum were excluded to account for the higher concentration of Cr and Cho [15] in the cerebellum. NAA, Cr, Cho, NAA/Cr, NAA/Cho of all so defined voxels of a lobe of interest were then analyzed as a function of white matter percentage using a linear regression analysis to calculate the mean metabolite intensity or ratio expected for given WM% in a voxel (M_{mean}) (cf. Fig. 2).

$$M_{mean}=b0+b_{wm}\cdot \%WM,$$

Where b0 represents the intercept, b_{wm} the slope of the regression line and %WM the percentage of white matter in a given voxel. This regression analysis was used to calculate the 95% prediction interval for an additional observation using the following formula:

$$M_{(p\leq\alpha)}=M_{mean}\pm t\,\alpha_{(n-2)}\cdot SE_{res}\cdot\sqrt{1+1/n+\frac{(\%WM-\%WM_{mean})^2}{(n-1)\cdot SD\%WM^2}},$$

where, M ($p \leq \alpha$): the threshold value corresponding to a p-value $\leq \alpha$ for metabolite intensity or ratio when $\alpha = 0.05$; t α (n-2): t-value for $p \leq \alpha$. for n-2 degrees of freedom; n: number of voxels; SE_{res}: residual standard error; %WM: percentage of white matter in the observed voxel; $\%WM_{mean}$: mean white matter percentage of control population; SD%WM: standard deviation of white matter percentage in the control population.

To account for a rostro-caudal gradient resulting in lower metabolite intensities in the lower slices, these thresholds were determined for every slice separately. Voxels with metabolite intensities or ratios outside the 95% prediction interval were considered to be "pathological".

In patients, all voxels in a lobe containing 50% or more "malformation" were selected. The representation of these voxels on the reference image closely corresponded to the MR visible lesion and they were therefore defined to represent the CM (cf. Fig. 3a). The "perilesional zone" was defined as all voxels in the same hemisphere as the malformation containing more than 1% but less than 50% "malformation". On the reference images, perilesional voxels selected by this definition were displayed in the structurally normal area adjacent to the structural lesion on the MRI (cf. Fig. 3b). All pathological voxels in the CM and the perilesional zone were then identified using the thresholds determined in the respective control group. The number of all pathological voxels in the CM and the perilesional zone was expressed as percentage of all voxels in the corresponding zone. The localization of those voxels defined as "pathological" in the CM and the perilesional zone was indicated on the corresponding MRI slice for anatomical reference. By definition, about 5% of all voxels in a subject, even in a control, will be identified as outside the 95% prediction interval for one parameter, e.g. NAA. Fig. 4a shows the typical distribution of all voxels that were outside one or several prediction intervals for a control subject. Fig. 4b–d shows the same for three patients. As can be seen

while the overall amount of these voxels is about the same (8–12%), the distribution of those voxels is rather diffuse in controls while there are clusters of abnormal voxels in the patients. Because the number of voxels in CM or a perilesional zone was small compared with the total number of all voxels in a dataset (CM: mean 4.9% (range 0.2–12.1%); perilesional zone: mean 8.7% (range 5–16.7%) and because not all voxels in the CM or the perilesional zone were pathological, the overall amount of pathological voxels in the patient group was not significantly increased compared to the control group.

In addition to this voxel-based type of analysis, we also performed a region of interest (ROI) analysis. In each patient, mean and standard deviation (SD) of all metabolites and metabolite ratios in voxels identified as “malformation” and “perilesion” were calculated. To allow for comparison with normal tissue, mean and SD of corresponding regions in controls, i.e. matched for gray/white matter content, lobe and slice, were calculated. Individual malformations or perilesional regions were identified as abnormal if their mean was outside the 2SD interval from the corresponding mean in controls.

Results

Table 1 displays the characteristics of the patients. The radiological diagnoses of the CMs were cortical dysplasia (n = 2), subependymal heterotopia combined with polymicrogyria with schizencephaly, (n = 4) isolated polymicrogyria (n = 1), and transmantle dysplasia (n = 3; all in patient 4). 519 voxels in these eight patients fulfilled the criteria for “malformation” and 995 for “perilesional zone”. 30% of the voxels fulfilling the criteria for “malformation” were identified as “pathological” by one or more of the metabolites or ratios. The percentage of pathological voxels in individual CMs varied between 0% and 78% (cf. Table 1). On the reference images most pathological voxels were displayed as clusters in gray matter regions that were generally smaller than the MRI visible lesion. There was no correlation between the size of the CM and percentage of pathological voxels. 36% of the voxels in cortical dysplasias (2 patients), 31% of the voxels in heterotopias in combination with polymicrogyria and schizencephaly (4 patients), 67% of the voxels in one of the transmantle dysplasias (1 patient) and 0% of the voxels in the isolated polymicrogyria (1 patient) were identified as pathological.

In the perilesional zone, 15% of all voxels were identified as pathological by one or more parameters. The percentage of pathological voxels in individual perilesional zones varied between 4% and 39% (cf. Table 1). On the reference images, pathological voxels were usually clustered and confined to a small part of the perilesional zone. Only a few, isolated voxels were located immediately adjacent to the MR visible lesion. There was no correlation between size of the “perilesional” zone and percentage of pathological voxels in this zone. Additionally, there was also no correlation between the percentage of pathological voxels in the CM and the percentage of pathological voxels in the “perilesional zone”.

Table 2 displays the mean percentage and range of pathological voxels in the different metabolic categories. The most frequent abnormalities of single metabolites in CMs were a decrease of NAA or an increase of Cho and consequently a decrease of NAA/Cr or NAA/Cho the most frequently abnormal ratios. A decrease of NAA or Cr and thus decreases or increases of NAA/Cr were the most frequently found abnormalities in the perilesional zone. The type of CM had no influence on the presence or absence of metabolic abnormalities in the perilesional zones.

Table 3 displays the metabolic abnormalities of individual CMs found in at least 10% or more of the voxels. There was no characteristic metabolic signature for the different types of CMs. While there was some overlap, i.e. regions where more than one parameter was abnormal,

different metabolic abnormalities usually affected different regions within the CM (cf. Fig. 5). The same was true for the perilesional zone (cf. Fig. 6).

Table 4a and 4b show the results of the ROI analysis. There was no difference between the two goups (cf Table 4a). In the individual analysis, significant metabolic abnormalities were found in three malformations and in two perilesional zones (cf. Table 4b). Because of the metabolic and regional heterogeneity found in the voxel-based analysis, the lower sensitivity of the ROI analysis had be expected.

Discussion

There were two major findings in this study: 1. The major metabolic abnormalities in CM were decreased NAA and increased Cho. Other abnormalities, e.g., increases or decreases of Cr were also observed, but less frequently. 2. CMs contained varying portions of metabolically normal and abnormal regions. 3. Metabolic abnormalities, usually decreased NAA and Cr, were also found in some areas of the macroscopically normal perilesional zone. As in the CMs, these metabolic abnormalities showed regional variations.

The first major finding is that CMs were most often characterized by decreased NAA and increased Cho. There were also regions with decreased or increased Cr, decreased Cho or regions with multiple metabolic abnormalities but those were less frequent.

NAA seems to be the most sensitive spectroscopic marker for metabolic disturbances associated with epilepsy. In medial temporal lobe epilepsy (mTLE), NAA is decreased in the epileptogenic focus and in regions involved in seizure spread, while Cr and Cho are usually normal [5,21]. While decreased NAA in mTLE is usually considered to represent loss of neuronal cells or neuronal dysfunction, a normal NAA is thought to indicate functionally normal neuronal tissue. Decreased NAA is also one of the most frequently found abnomalies in CM. However, CM are characterized by a disorganization of tissue architecture and may contain immature and even undifferentiated cells. Structural abnormalities are usually also associated with functional abnormalities. A disorganized tissue architecture, for example, may complicate cell-to-cell interactions, e.g., the transport of NAA from neurons to glial cells where it is hydrolyzed by amidohydrolase [2,7]. Furthermore, immature or undifferentiated cells have different metabolic properties than mature cells, e.g. contrary to mature glial cells, immature glial cells are able to synthesize NAA [3,30]. Therefore, metabolic abnormalities in CMs are probably quite complex and diverse and the assumptions regarding the nature of the metabolic abnormalities in mTLE are unlikely to be valid in CMs. This hypothesis is also supported by their other characteristics, i.e., regional variability within the CM and additional abnormalities of Cho and Cr.

The second major finding of this study is that CM were metabolically heterogeneous. In addition to metabolically abnormal regions, they may contain large metabolically normal areas as only 30% of all voxels fulfilling the criteria for “malformation” were identified as “pathological”. The extent to which structural abnormalities in individual CMs were associated with metabolic abnormalities varied between 0–78%. Typically, metabolically abnormal areas were smaller than the structural abnormalities on MRI in which they were represented as metabolically heterogeneous clusters of abnormal voxels surrounded by metabolically normal regions. The high percentage of normal voxels may partly reflect the definition of “malformation” used in this study, which included not only tissue from the CM proper, e.g., a heterotopic nodule, but also the overlaying cortical gray matter or surrounding white matter if appearing abnormal on the MRI. The latter two contain probably mostly mature glial and neuronal cells and the tissue architecture is normal or only slightly disturbed [1]. Therefore, metabolic abnormalities in such regions might be absent or very subtle. Furthermore, it has to

be considered that the signal originating from a spectroscopy voxel also has contributions from adjacent voxels due to the characteristic point spread function associated with phase encoding. Owing to this partial volume effect, adjacent metabolically normal voxels outside the CM could affect abnormalities in voxels in the CM. This effect would particularly affect voxels at the border to structurally normal tissue which contain already by definition up to 50% structurally normal tissue. However, while such methodological issues may explain the existence of normal voxels in border zones of CMs, they do not explain why one CM was completely metabolically normal or why the reference images showed clusters of metabolically normal areas also to occur within the CM proper of other patients. They also cannot explain why abnormal areas in CM were metabolically heterogeneous, i.e., why different regions of the same CM showed different types of abnormalities, e.g. low NAA in one part and high Cho in another part. Thus, we conclude that metabolic heterogeneity and the absence of metabolic abnormalities in CM regions with clearly disturbed cytoarchitecture are probably features inherent to the CM itself. To our knowledge, the occurrence of metabolically normal regions together with metabolically abnormal regions in CM has not been reported hitherto.

The third major finding was that metabolic abnormalities were also found in the normal appearing tissue surrounding the CM. As pointed out in the previous paragraph, this could be due to partial voluming, but in this case due to a contribution from severe abnormalities within the CM to metabolically normal voxels in the perilesional zone. However, perilesional abnormalities due to partial voluming would be expected to have a metabolic pattern similar to the CM and to be located adjacent to the abnormalities within the CM. Since the majority of the pathological perilesional voxels did not fulfill these criteria, we conclude that those metabolic abnormalities are not due to a partial volume effect but represent true metabolic abnormalities in the perilesional zone.

Perilesional spectroscopic abnormalities have been previously reported [4,31], and two PET studies also showed perilesional changes [16,12]. Previous MRS studies found perilesional alterations to be less severe than those in the CM, a finding that would be consistent with partial voluming. However, contrary to this study, both previous studies compared the averages of all voxels of one zone with the average from the other zone, thereby probably mixing metabolically abnormal voxels with normal voxels. If there are more metabolically abnormal voxels in the CM than in the perilesional zone, as found in our study, averaging also results in a gradient between the two zones. Therefore, it cannot be excluded that the finding of less severe metabolic abnormalities in the perilesional zone in the two previous studies might be a methodological artifact. A further disadvantage of averaging is that information about the spatial distribution of the abnormalities, which may be of clinical importance, is lost.

There are three possible causes of metabolic abnormalities in the perilesional zone. First, perilesional abnormalities might represent areas with normal tissue architecture but intrinsic epileptic activity due to aberrant connections. This hypothesis is supported by findings of a PET study [16] where perilesional areas with abnormal flumazenil binding showed interictal spiking during intraoperative electrocorticography. Second, perilesional abnormalities might represent microscopic abnormal brain regions, e.g., small clusters of heterotopic neurons in otherwise normal white matter regions. If associated with abnormal connections to other brain regions, such subtle abnormalities can eventually promote the spread of paroxysmal activity to other brain regions [8,23]. In both cases, the presence or absence of perilesional metabolic abnormalities and their location in relation to the CM might be of clinical interest, particularly in patients in whom a surgical intervention is being considered. This would not apply to the third possible explanation, i.e., that metabolic abnormalities in the perilesional zone simply reflect the involvement of the otherwise histologically and functionally normal perilesional tissue in seizure spread. However, the fact, that not only NAA but also Cr and Cho have been found to be abnormal in the perilesional zone argues against this explanation because it has

been shown in TLE that regions secondarily involved in seizure spread are typically characterized by NAA reductions but normal Cr and Cho [15].

This study has limitations: 1. The population studied was rather small and included malformations of different severity, i.e., malformations due to abnormal glial and neuronal proliferation and apoptosis as well as malformations due to abnormal cortical organization. 2. Because we used a long echo time, we might have missed abnormalities of glutamate or myo-inositol. Abnormalities of those metabolites in CM have been described by others [31]. 3. The acquisition protocol was designed to study the accuracy of focus localization in NE by MRSI. The MRSI slices were positioned in a standardized manner and no attempt was made to adapt the positioning to allow for a complete coverage of the CM and the perilesional zone in each subject. Therefore, potentially clinically important information might have been lost. A 3D MRSI sequence, which covers the whole brain, might be a better technique to study these patients. 4. In addition to metabolite ratios we also calculated metabolite intensities but did not correct for variation of peak intensities due to coil inhomogeneities and susceptibility artifacts. However, the findings for metabolite intensities were generally in good agreement with the findings for ratios and thus these effects were probably negligible. Nonetheless, if this method is applied for the analysis of larger brain areas, it is advisable to use ratios. Since NAA and Cho were most often abnormal in CMs, a combination of NAA/Cr and NAA/Cho would eventually describe them best. 5. Since we did not test for alterations of T1 and T2 relaxation characteristics in CMs, we cannot exclude that the metabolic abnormalities observed in CM might be partially or even entirely caused by such effects. 6. By using ratios and metabolite intensities and exploring for positive and negative deviations from the norm, we maximized the possibility of finding abnormal voxels. This was partly done intentionally, because it was our aim to demonstrate that metabolically completely normal areas are interspersed with metabolically abnormal areas. However, this also means that the abnormal findings should be critically assessed.

In conclusion, the most frequent abnormality in CMs is a decrease of NAA and an increase of Cho, but alterations of other metabolites with regional variability can also be found. CMs contain metabolically normal and abnormal regions side by side. Perilesional metabolic abnormalities have similar metabolic characteristics as CMs and may therefore have intrinsic epileptogenicity.

Acknowledgments

The authors thank Drs. D. G. Vossler, R. C. Knowlton from the Swedish Epilepsy Center of the University of Washington, Seattle and Dr M. C. Salinsky from the Oregon Health Sciences University Epilepsy Center, Portland, Oregon for the referral of some of their patients for this study.

This work was supported by NIH grant ROI-NS31966 (K. D.L) S. G.M was supported by a Grant from the Swiss National Science Foundation.

References

1. Battaglia G, Arcelli P, Granata T, et al. Neuronal migration disorders and epilepsy: a morphological analysis of three surgically treated patients. Epilepsy Res 1996;26:49–58. [PubMed: 8985686]
2. Bhakoo KK, Craig TJ, Styles P. Developmental and regional distribution of aspartoacylase in rat brain tissue. J Neurochem 2001;79:211–220. [PubMed: 11595773]
3. Bhakoo KK, Pearce D. In vitro expression of N-acetylaspartate by oligodendrocytes: Implications for proton magnetic resonance spectroscopy signal in vivo. J Neurochem 2000;74:254–262. [PubMed: 10617127]
4. Boonyapisit K, Najm I, Klem G, et al. Epileptogenicity of focal malformations due to abnormal cortical development: direct electrocorticographic-histopathologic correlations. Epilepsia 2003;44:69–76. [PubMed: 12581232]

5. Capizzano AA, Vermathen P, Laxer KD, et al. Multisection proton MR spectroscopy for mesial temporal lobe epilepsy. Am J Neuroradiol 2002;23:1359–1368. [PubMed: 12223379]
6. Castillo M, Kwock L, Scatliff J, Gudeman S, Greenwood R. Proton MR spectroscopic characteristics of a presumed giant subcortical heterotopia. Am J Neuroradiol 1993;14:426–429. [PubMed: 8456723]
7. Chakraborty G, Mekala P, Yahya D, Ledeen RW. Intraneuronal N-acetylaspartate supplies acetyl groups for myelin lipid synthesis: evidence for myelin-associated aspartoacylase. J Neurochem 2001;78:736–745. [PubMed: 11520894]
8. Chevassus-au-Louis N, Represa A. The right neuron at the wrong place: biology of heterotopic neurons in cortical migration disorders with special reference to associated pathologies. Cell Mol Life Sci 1999;55:1206–1215. [PubMed: 10487203]
9. Damasio, H. Human brain anatomy in computerized images. Oxford University Press; New York: 1995.
10. Grant PE, Barkovich AJ, Wald LL, Dillon WP, Laxer KD, Vigneron DB. High resolution surface-coil MR of cortical lesions in medically refractory epilepsy: a prospective study. Am J Neuroradiol 1997;18:291–301. [PubMed: 9111666]
11. Guye M, Le Fur Y, Confort-Gouny S, et al. Metabolic and electro-physiological alterations in subtypes of temporal lobe epilepsy: a combined proton magnetic resonance spectroscopic imaging and depth electrode study. Epilepsia 2002;43:1197–209. [PubMed: 12366736]
12. Hammers A, Koepp MJ, Richardson MP, et al. Central benzodiazepine receptors in malformations of cortical development. A quantitative study. Brain 2001;124:1555–1565. [PubMed: 11459747]
13. Hanefeld F, Kruse B, Holzbach U, et al. Hemimegalencephaly: localized proton magnetic resonance spectroscopy in vivo. Epilepsia 1995;36:1215–1224. [PubMed: 7489699]
14. Haupt CI, Schuff N, Weiner MW, Maudsley AA. Removal of lipid artifacts in ^{1}H spectroscopic imaging by data extrapolation. Magn Reson Med 1996;35:678–687. [PubMed: 8722819]
15. Jacobs MA, Horská A, van Zijl PCM, Barker PB. Quantitative proton MR spectroscopic imaging of normal human cerebellum and brain stem. Mag Reson Med 2001;46:699–705.
16. Juhász C, Chugani DC, Muszik O, et al. Electroclinical correlates of flumazenil and fluorodeoxyglucose PET abnormalities in lesional epilepsy. Neurology 2000;55:825–834. [PubMed: 10994004]
17. Kuzniecky R, Hetherington H, Pan J, et al. Proton spectroscopic imaging at 4.1 T in patients with malformations of cortical development and epilepsy. Neurology 1997;48:1018–1024. [PubMed: 9109893]
18. Li LM, Cendes F, Cunha Bastos A, Andermann F, Dubeau F, Arnold DL. Neuronal metabolic dysfunction in patients with cortical developmental malformations. Neurology 1998;50:755–759. [PubMed: 9521269]
19. Marsh L, Lim KO, Sullivan EV, Lane B, Spielman D. Proton magnetic resonance spectroscopy of a gray matter heterotopia. Neurology 1996;47:1571–1574. [PubMed: 8960748]
20. Maudsley AA, Lin E, Weiner MW. Spectroscopic imaging display and analysis. Magn Reson Imag 1992;10:471–485.
21. Mueller SG, Suhy J, Laxer KD, et al. Reduced extrahippocampal NAA in mesial temporal lobe epilepsy. Epilepsia 2002;43:1210–1216. [PubMed: 12366737]
22. Najm I, Ying Z, Babb T, et al. Mechanisms of epileptogenicity in cortical dysplasias. Neurology 2004;62 (6 Suppl 3):S9–S13. [PubMed: 15037672]
23. Palmini A. Disorders of cortical development. Curr Opin Neurol 2000;13:183–192. [PubMed: 10987577]
24. Porter BE, Brooks-Kayal A, Golden JA. Disorders of cortical development and epilepsy. Arch Neurol 2002;59:361–365. [PubMed: 11890838]
25. Schuff N, Ezekiel F, Gamst AC, et al. Region and tissue differences of metabolites in normally aged brain using multislice ^{1}H magnetic resonance spectroscopic imaging. Mag Reson Med 2001;45:899–907.
26. Simone IL, Federico F, De Blasi R, et al. Metabolic changes in neuronal migration disorders: evaluation by combined MRI and Proton MR spectroscopy. Epilepsia 1999;40:872–879. [PubMed: 10403210]

27. Soher BJ, Young K, Govindaraju V, Maudsley AA. Automated spectral analysis III: Application to in vivo proton MR spectroscopy and spectroscopic imaging. Magn Reson Med 1998;40:822–831. [PubMed: 9840826]

28. Tanabe JL, Amend D, Schuff N, et al. Tissue segmentation of the brain in Alzheimer disease. Am J Neuroradiol 1997;18:115–123. [PubMed: 9010529]

29. Tassi L, Pasquier B, Minotti L, et al. Cortical dysplasia: electroclinical, imaging and neuropathologic study of 13 patients. Epilepsia 2001;42:1112–1123. [PubMed: 11580757]

30. Urenjak J, Williams SR, Gadian DG, Noble M. Specific expression of N-acetylasparate in neurons, oligodendrocyte-type-2 astrocyte progenitors and immature oligodendrocytes in vitro. J Neurochem 1992;59:55–61. [PubMed: 1613513]

31. Woermann FG, McLean MA, Bartlett PA, Barker GJ, Duncan JS. Qualitative short echo time proton magnetic resonance spectroscopic imaging study of malformations of cortical development causing epilepsy. Brain 2001;124:427–436. [PubMed: 11157569]

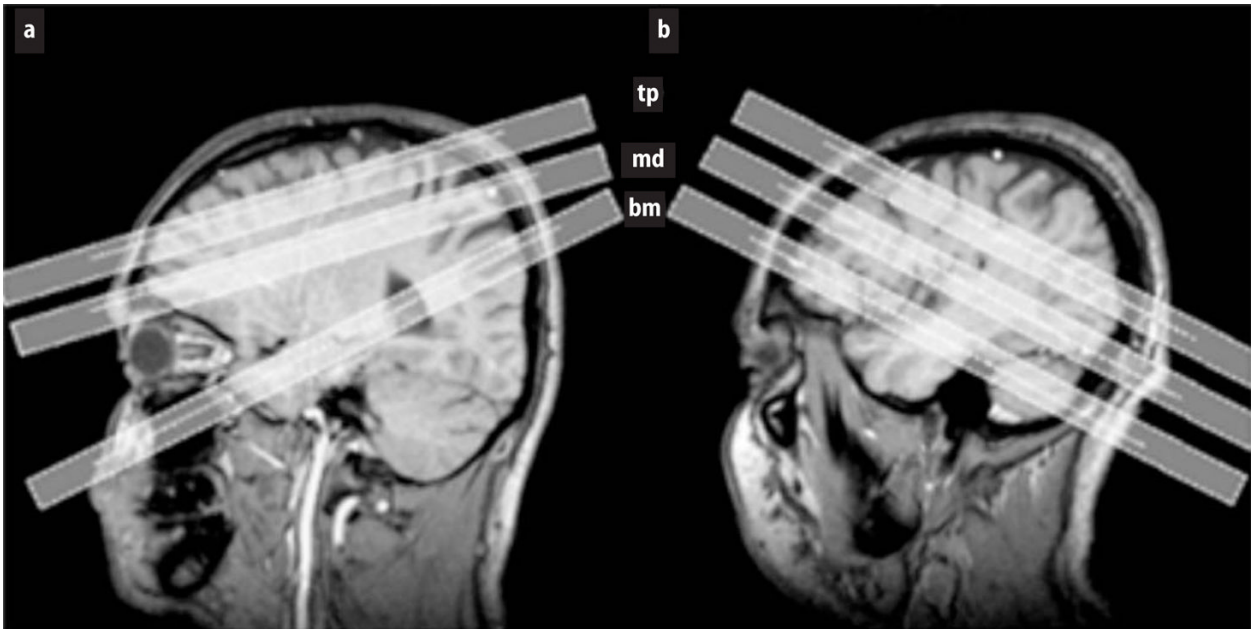

Fig. 1.
T1 weighted images demonstrating the position of the three MRSI slices in (**a**) the "old protocol" and (**b**) in the "new protocol (*bm* bottom or hippocampal slice; *md* "middle" or ventricular slice; *tp* top or supraventricular slice)

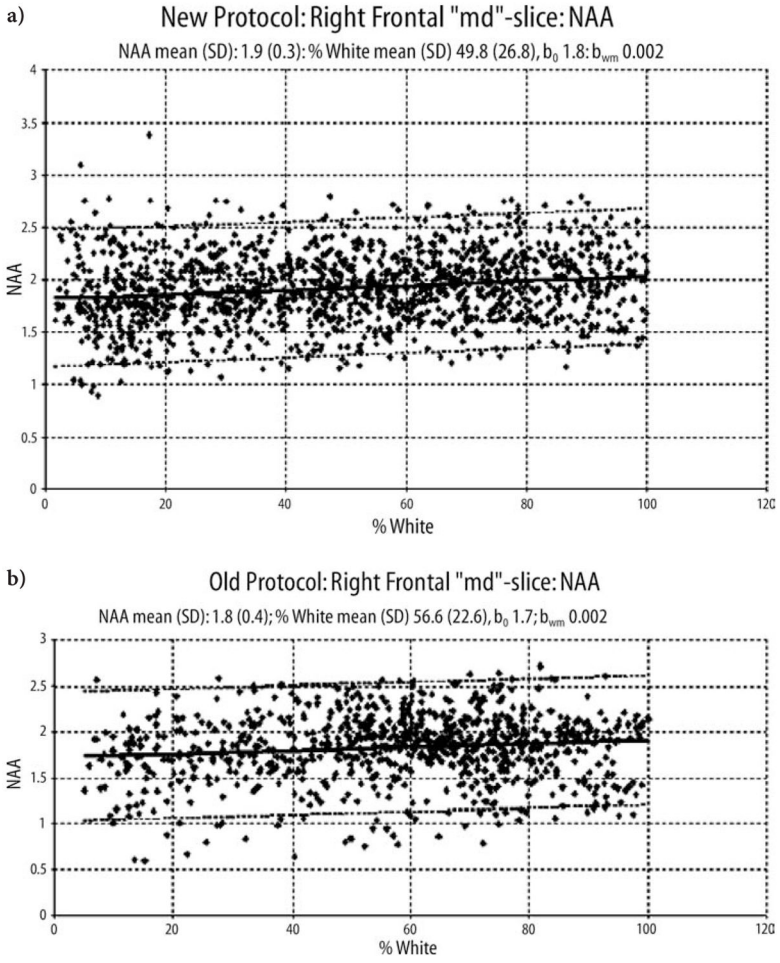

Fig. 2.

a. Linear regression plots of NAA of the right frontal lobe from the middle slice of the control group as a function of white matter percentage for the "new" protocol. **b.** For the "old" protocol. The dashed line indicates the 95 % confidence interval.

b_0, intercept; b_{wm}, slope of the regression function.

The regression plots show that NAA is higher in white matter than in gray matter. The reasons for this finding are discussed in depth in the paper of Schuff et al. [25].

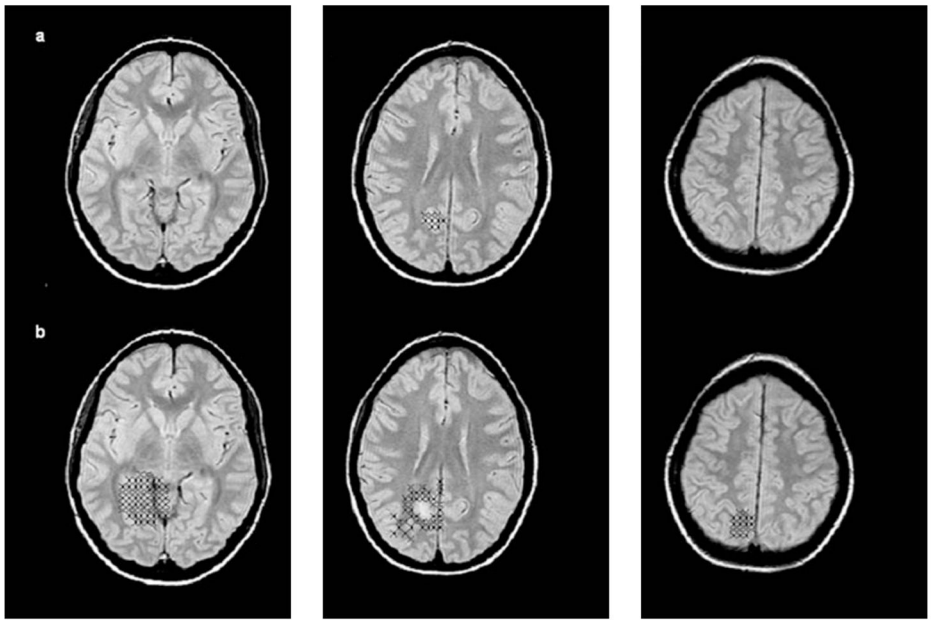

Fig. 3.
(**a**) All voxels containing 50% or more “lesion” in patient 9, i.e, voxels representing the malformation. (**b**) All voxels containing ≥1% but ≤50% “malformation”, i.e. voxels representing the perilesional zone

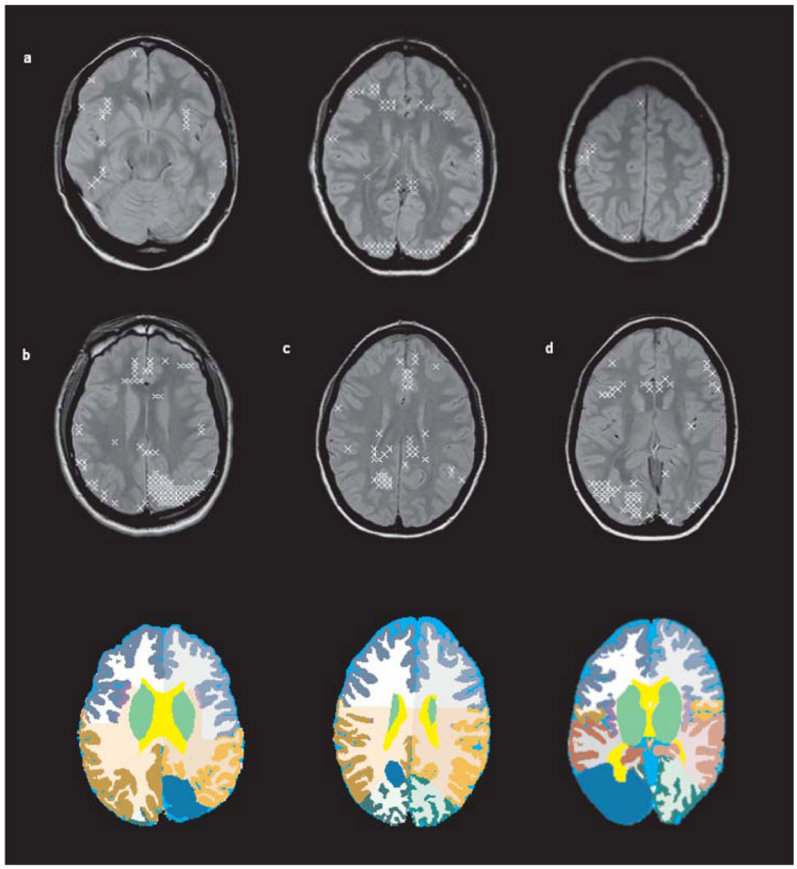

Fig. 4.

(**a**) Abnormality map, i.e., spatial distribution of all voxels outside one or several of the five different 95 % prediction intervals (NAA, Cr, Cho, NAA/Cr, NAA/Cho) in a control. The distribution of those voxels is rather diffuse. (**b**) Abnormality map for patient No1 and below, region of the malformation indicated in blue in the left parietal lobe on the segmentation image. As can be seen, abnormal voxels tend to cluster in the region of the malformation. (c) Abnormality map with corresponding segmentation slice for patient No 7 and (d) for patient No 5

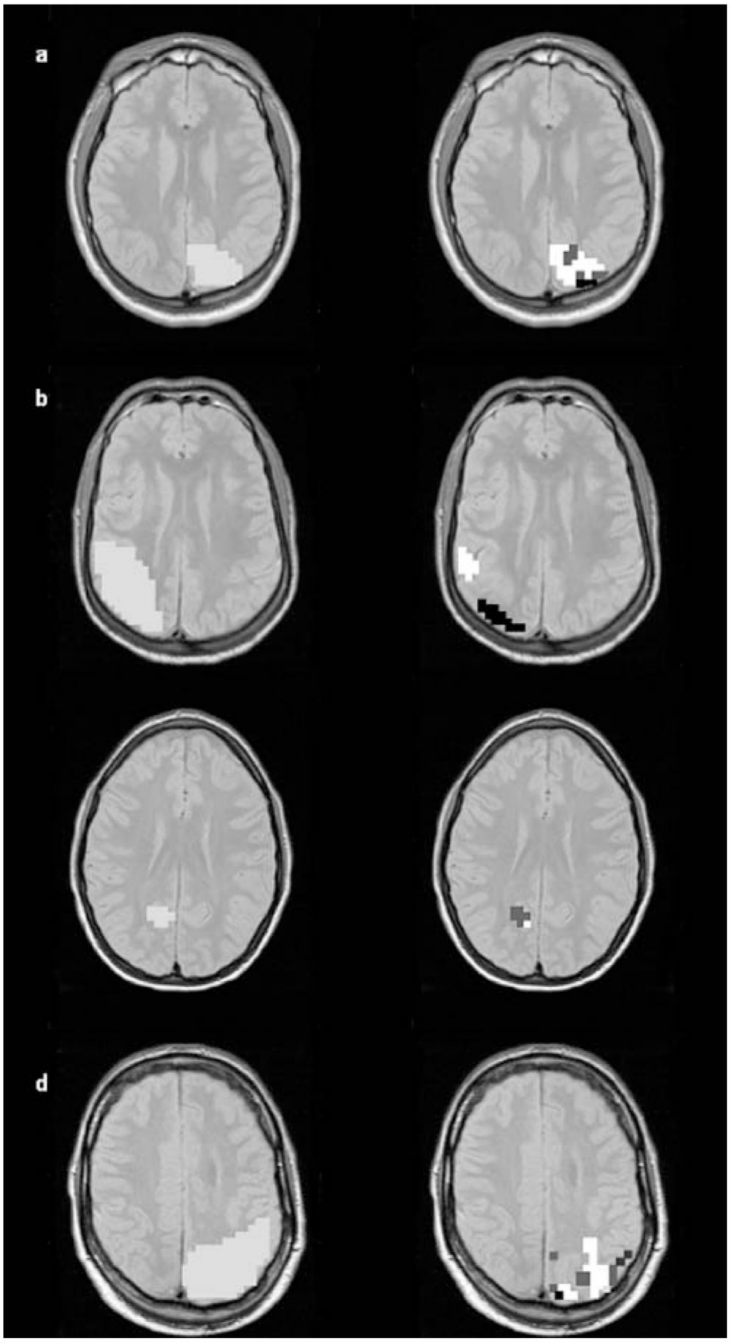

Fig. 5.

Spatial distribution of metabolic abnormalities in cortical malformations. Left side: All voxels fulfilling the criteria for “malformation” indicated by pale gray squares on the MRSI slice with the best coverage of the malformation. On the right side, voxels outside the 95 % prediction interval. (**a**) Patient 1: “Middle slice”: Right side: Black squares: decreased NAA; white squares: increased Cho; dark gray: decreased NAA and increased Cho. (**b**) Patient 3. “Middle slice”: Right side: Black squares: decreased NAA; white squares: decreased NAA/Cr. (**c**) Patient 7: “Middle slice”: Right side: White squares: increased Cho; dark gray: increased Cho and decreased NAA/Cr. (**d**) Patient 8: “Middle slice”: Right side: Black square: NAA decreased; white squares: Cho decreased; dark gray: Cr increased; middle gray: two of three,

i.e. NAA, Cr or Cho changed. Changes of NAA/Cr, NAA/Cho were also found in this patient but are not indicated

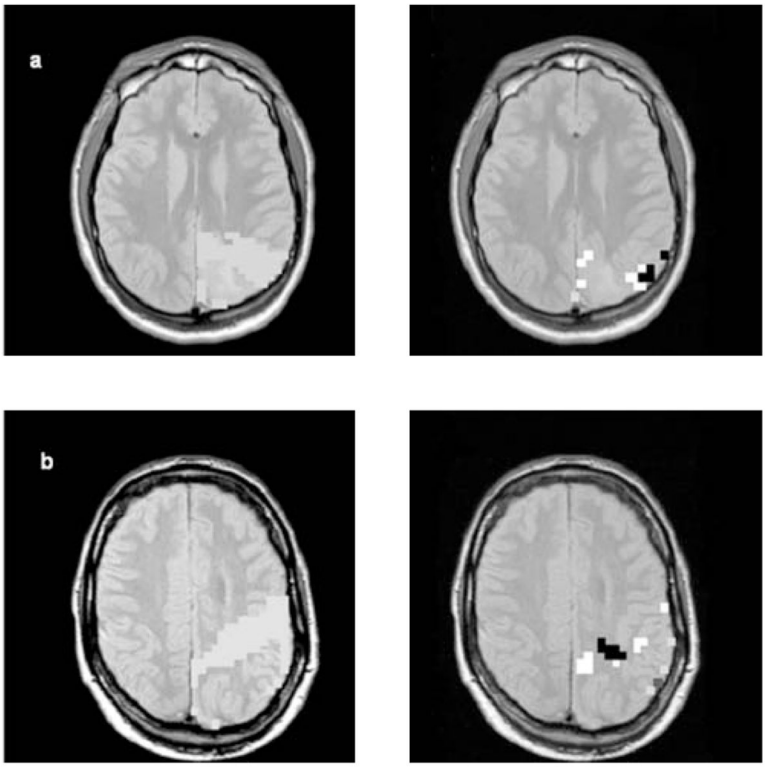

Fig. 6.

Spatial distribution of metabolic abnormalities in the perilesional zone. Left side: All voxels fulfilling the criteria for “perilesion” indicated by pale gray squares on the MRSI slice with the best coverage of the perilesional zone. On the right side, voxels outside the 95 % prediction interval. (**a**) Patient 1: “Middle slice”: Right side: Black squares: decreased NAA; white squares: decreased NAA/Cho; pale gray: decreased Cr. (**b**) Patient 8: “Middle slice”: Right side: Black squares:NAA/Cr increased; white squares: Cho decreased; dark gray: Cr and Cho decreased; pale gray: Cr decreased

Table 1

Patients Characteristics

Patient No	Gender/Age at Examination	EEG Focus	Cortical Malformation	% Path MRSI Voxels in Lesion	% Path MRSI Voxels Perilesion
1	M/19	L FP	L POT subependymal heterotopia, polymicrogyria with schizencephaly	63.0	20.0
2	F/32	L F	L TO cortical dysplasia	26.0	14.0
3	M/35	R TP	R TP subependymal heterotopia, polymicrogyra with schizencephaly	20.0	9.0
4	M/17	L + R F	R F transmantle dysplasia	67.0	20.3
			L P transmantle dysplasia	na	11.4
			R P transmantle dysplasia	na	42.1
5	F/31	R TO	R TO subependymal heterotopia and polymicrogyria	26.0	4.0
6	F/16	L TO	L TOP polymicrogyria	0.0	23.0
7	F/23	R O	R OPT focal cortical dysplasia	78.0	11.0
8	M/37	L PO	L TPO subependymal heterotopia, polymicrogyria with schizencephaly. Dandy-Walker-syndrome	36.0	28.0

M male; *F* female; *L* left; *R* right; *F* frontal; *T* temporal; *P* parietal; *O* occipital; *na* very small malformation hence no voxel fulfilling 50 % criterion % Path MRSI Voxels: Number of “pathological” MRSI voxels expressed as percentage of all voxels in “lesion”, respectively “perilesion”

J Neurol. Author manuscript; available in PMC 2009 July 13.

Table 2

Metabolical Abnormalities in Pathological MRSI Voxels: Mean Percentage and (Range) of Voxels with Abnormality

	NAA ↓	**NAA ↑**	**Cr ↓**	**Cr ↑**	**Cho ↓**	**Cho ↑**	**NAA/Cr ↓**	**NAA/Cr ↑**	**NAA/Cho ↓**	**NAA/Cho ↑**
Malformation	13.0 (0–66.7)	0.4 (0.0–2.2)	5.2 (0.0–33.3)	3.0 (0.0–11.1)	3.4 (0.0–27.0)	15.2 (0.0–77.8)	13.3 (0.0–49.1)	2.2 (0.0–10.0)	10.6 (0.0–57.6)	3.3 (0.0–13.3)
Perilesional Zone	3.4 (0.0–15.0)	1.0 (0.0–7.6)	3.0 (0.0–18.3)	0.7 (0.0–4.8)	1.1 (0.0–10.0)	1.0 (0.0–7.1)	3.2 (0.0–11.4)	8.4 (0.0–42.1)	1.9 (0.0–7.8)	1.2 (0.0–6.4)

Percentage of voxels with abnormality, number of all voxels of all subject with e.g. NAA↓ in a region, e.g. malformation, expressed as percentage of all voxels of all subjects in the region

↓, below the 95 % prediction interval; ↑, above the 95 % prediction interval; *NAA* N-acetylaspartate; *Cr* creatine/phosphocreatine; *Cho* choline compounds Definition of “perilesional” see text

J Neurol. Author manuscript; available in PMC 2009 July 13.

Table 3

Most Prominent Metabolical Abnormalities Found in Individual Patients

Patient No	Radiological classification	Metabolic Abnormality	
		Malformation	**Perilesional zone**
1	heterotopia, polymicrogyria	**NAA/Cho** ↓, NAA ↓, Cho ↑, NAA/Cr ↓	minor
2	cortical dysplasia	**NAA/Cr** ↓*	**NAA/Cr** ↓*
3	heterotopia, polymicrogyria	**NAA** ↓	minor
4	R F transmantle dysplasia	**NAA** ↓, Cr ↓	**Cr** ↓, NAA/Cr ↑
	L P transmantle dysplasia	na	**NAA/Cr** ↑*
	R P transmantle dysplasia	na	**NAA/Cr** ↑
5	heterotopia, polymicrogyria	**NAA/Cho** ↑*, NAA/Cr ↑*	minor
6	polymicrogyria	no	**NAA** ↓
7	cortical dysplasia	**Cho** ↑, NAA/Cr ↓, NAA/Cho ↓, Cr ↑	minor
8	heterotopia, polymicrogyria	**Cho** ↓, NAA/Cho ↑, NAA ↓	**Cho** ↓

prominent, more than 10 % of the voxels with metabolic abnormality

*1–9 % of voxels with isolated pathological NAA, Cr and Cho

NAA N-acetylaspartate; *Cr* creatine/phosphocreatine; *Cho* choline compounds; *Ipsi* hemisphere with malformation; *no* normal; *na* non available; *minor* minor abnormalities, i.e., different abnormalities none affects 10 % or more of the voxels

bold metabolic abnormality with highest percentage of voxels

↓, decrease; ↑ increase

Table 4

Table 4a Region of Interest Analysis: Group Mean and SD of metabolites and GM

Group	Region	% GM in ROI Mean (SD)	NAA Mean (SD)	Cr Mean (SD)	Cho Mean (SD)	NAA/Cr Mean (SD)	NAA/Cho Mean (SD)
Controls	Mixed GM + WM for Lesion	39.49 (13.17)	1.68 (0.18)	0.82 (0.05)	0.21 (0.03)	2.09 (0.22)	8.76 (1.66)
	Mixed GM + WM for Perilesion	38.45 (12.75)	1.67 (0.16)	0.78 (0.06)	0.22 (0.04)	2.22 (0.16)	8.59 (1.99)
Patients	Lesion	39.85 (15.49)	1.51 (0.28)	0.74 (0.19)	0.20 (0.07)	2.11 (0.41)	8.24 (2.45)
	Perilesion	34.24 (12.19)	1.52 (0.32)	0.74 (0.19)	0.21 (0.07)	2.12 (0.54)	8.82 (5.11)

Table 4b ROI: Significant Metabolical Abnormalities Found in Individual Patients

Patient No	Radiological classification	Metabolic Abnormality	
		Malformation	Perilesional zone
1	heterotopia, polymicrogyria	**NAA ↓, NAA/Cr ↓**	no
2	cortical dysplasia	no	**NAA/Cr ↓**
3	heterotopia, polymicrogyria	no	no
4	R F transmantle dysplasia	**NAA ↓**	no
	L P transmantle dysplasia	na	no
	R P transmantle dysplasia	na	no
5	heterotopia, polymicrogyria	no	**NAA ↓**
6	polymicrogyria	no	no
7	cortical dysplasia	**Cho ↑**	no
8	heterotopia, polymicrogyria	no	no

Mixed GM + WM: Voxels in controls were selected to match lobe and tissue composition of the malformation and perilesional region of each patient

There were no differences between the groups. NAA lesion showed a tendency to be lower (p = 0.06)

significant; 2 SD below or above mean in corresponding regions (lobe and matched for tissue composition) of controls

no within control range; *na* not available

J Neurol. Author manuscript; available in PMC 2009 July 13.